An Adaptive Power Sharing Control for Management of DC Microgrids Powered by Fuel Cell and Storage System

Aguiar, C. R.; Fuzato, G. F.; Machado, R. Q. Quadros; Guerrero, J. M.

Published in:
IEEE Transactions on Industrial Electronics

DOI (link to publication from Publisher):
10.1109/TIE.2019.2916312

Publication date:
2020

Document Version
Accepted author manuscript, peer reviewed version

An Adaptive Power Sharing Control for Management of DC Microgrids Powered by Fuel Cell and Storage System

Cassius R. Aguiar, Guilherme H. F. Fuzato, Ricardo Q. Machado, *Member, IEEE,* and Josep M. Guerrero, *Fellow, IEEE*

Abstract **- This paper presents an adaptive power-sharing methodology for management of dc microgrids powered by fuel cell (FC) and storage system (SS). In this context, the use of an adaptive *k*-sharing function in the control scheme is proposed to compensate the fast transients on the ac-side and manage the power sharing at steady-state regime between the FC and SS. The adaptive *k*-sharing is implemented with a low-pass filter transfer function for the FC and a complementary transfer function associated with the adaptive *k*-sharing gain for the SS. The proposed adaptive *k*-sharing function links the FC and the SS dynamics with the management of the dc microgrid, ensuring that the entire FC operation is performed in accordance with its operational limits. One of the main advantages of the proposed adaptive *k*-sharing is to reach high levels of stability and minimum disruptions on the FC terminals. To evaluate the feasibility of the proposed approach, we analyze the *k*-sharing behavior to determine the operational limits of the dc microgrid. Finally, to support the theoretical analysis we carried out a set of experimental results.**

Index Terms **- Fuel cells, dc/dc power converters, interconnected systems**.

I. INTRODUCTION

IN dc microgrids, the use of storage system (SS) reduces the intermittency of renewable energy sources dependent on the environmental conditions. In this solution, the use of fuel cells (FCs) as a main source is more attractive because they are supplied by hydrogen, and its power production is not affected by the sun irradiation or wind speed as in classical renewable energy sources [1], [2].

Manuscript received September 23, 2018; revised December 18, 2018; accepted April 22, 2019. This work was supported in part by the FAPESP under Grants 2016/25017-1, 2016/21120-2, 2013/20721-4, 2013/09788-0, and 2012/12770-2, and in part by CAPES under Grant 88881.030370/2013-01.

C. R. de Aguiar is with the Federal University of Technology - Paraná, Toledo PR 85902-490, Brazil (e-mail: cassiusaguiar@utfpr.edu.br).
G. H. F. Fuzato is with the Federal Institute of Education, Science and Technology of São Paulo, Campinas SP 01109-010, Brazil (e-mail: guilhermefuzato@ifsp.edu.br).
R. Q. Machado is with the São Carlos School of Engineering, University of São Paulo, São Carlos SP 13566-590, Brazil (e-mail: rquadros@sc.usp.br).
J. M. Guerrero is with the Department of Energy Technology, Aalborg University, Aalborg 9220, Denmark (e-mail: joz@et.aau.dk).

Unfortunately, FCs are characterized by low-voltage and high-current with slow dynamic response (around seconds or minutes), i.e. the control structure to manage the microgrid has an important role to prevent FC collapse, while the SSs present a faster dynamical response to block the instabilities produced on the ac-side [3], [4].

Considering the aforementioned drawbacks, many papers have discussed the use of FC in microgrids. In the most of them, the FCs are a part of the dc microgrid where the use of SSs, PV arrays and wind generators improve the system stability, capability of power production and power quality, respectively. Additionally, this type of solution is known as hybrid integration and it can be connected to the main grid or operate in standalone mode [5], [6].

Regarding the FC control structure, in general, two basic strategies have been used to compensate the FC dynamics, one with the direct control of the reactants, and another with the management of SSs. In the first, the goal is the direct control of fuel (flux of hydrogen and oxygen), where the hydrogen pressure control is the main technique applied to prevent fuel starvation [7], [8]. However, the main disadvantage of this method is the delay time of the mechanical devices (compressors, fans and valves) to regulate the fuel flux.

On the other hand, in the second strategy, the use of SSs provides the dc microgrids the capability to supply rapid transients, while the FCs, PV arrays and wind generators are in-charge of the steady-state regime [9]–[11].

In other studies, many centralized, decentralized, and hierarchical control methods have been proposed to manage and control dc microgrids [12]–[16]. The two main methods found are: droop based methods and active current-sharing methods. Droop based methods can be applied by means of a virtual resistance related to the dc-link voltage. A key feature of this method is that it does not need a communication link between the generation units. In contrast, active current-sharing methods use a low-bandwidth communication (LBC) to improve the performance of the dc microgrid operation.

However, the literature shows that most of the papers published present a general strategy to achieve power sharing in dc microgrids such as in [17]–[25]. In [17], the authors

This article has been accepted for publication in a future issue of this journal, but has not been fully edited. Content may change prior to final publication. Citation information: DOI 10.1109/TIE.2019.2916312, IEEE Transactions on Industrial Electronics

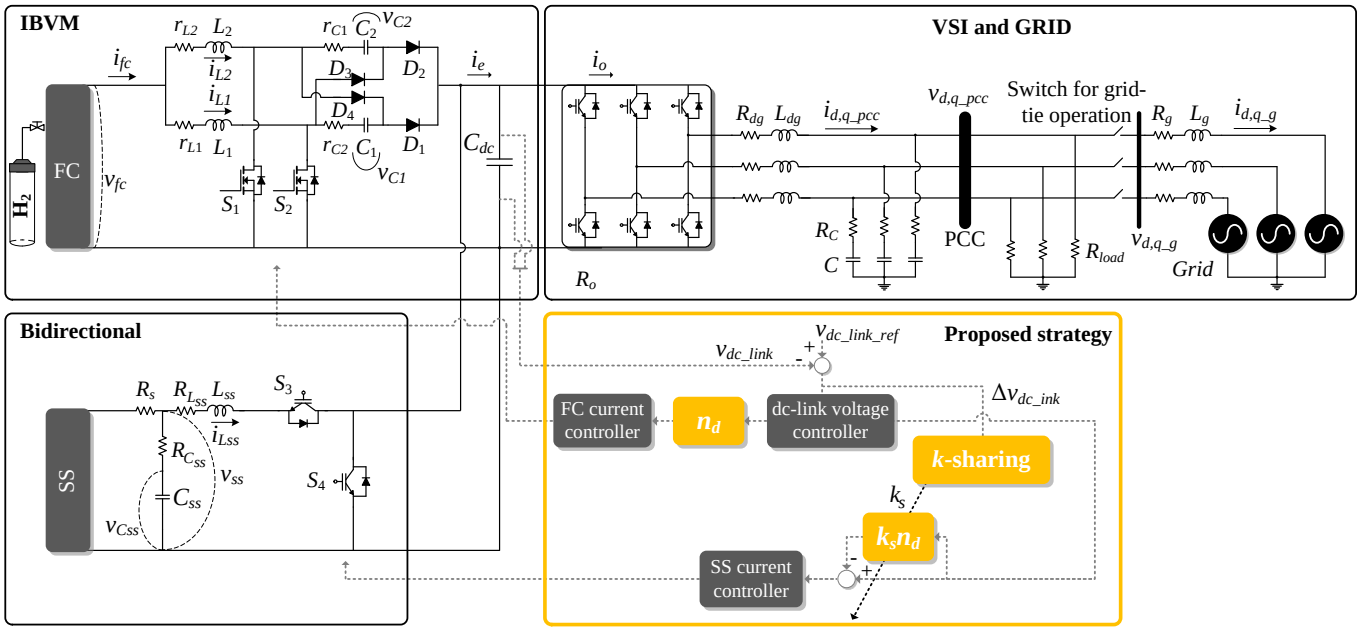

Fig. 1. Typical scheme for power-sharing.

develop a decentralized coordination control strategy that applies V–I droop concept to cooperate multiple PV sources in a dc microgrid. Moreover, an extended droop control (EDC) strategy to achieve dynamic current sharing autonomously during load maneuver and source variations is proposed in [19], and a voltage control that combines fuzzy logic with gain-scheduling techniques to accomplish both power sharing and energy management is presented in [20]. Lastly, a hierarchical active power management strategy for microgrids, including a fuel cell power conversion system, is described in [21].

In this context, the main difference of the proposed approach, as well as the papers published in the literature, is: in the proposed technique, we designed an adaptive *k*-sharing function, which suppresses the fast transients at the FC terminals to comply with FC slow dynamics related to the aforementioned delay time of mechanical devices. In this scenario, the system stability is improved by using a SS operating with complementary dynamics. In addition, the adaptive *k*-sharing includes the capability to manage the power sharing at steady-state and transitory regimes, widely controlling the dc-link over/under voltage.

This paper is organized as follow: in section II we present the system description. In section III the *k*-sharing description. In section IV we evaluate the adaptive *k*-sharing in terms of stability, while in section V we discuss the main results to prove the theoretical analysis. Finally, in section VI we conclude the proposed approach.

II. System Description

In Fig. 1 we show an interleaved boost with voltage multiplier (IBVM) converter powered by a fuel cell and a bidirectional buck-boost converter driven by a SS. To connect the dc microgrid to the main feeder, we use a voltage source inverter (VSI) controlled in the current (synchronous reference frame) mode and synchronized to the grid by means of a phase looked-loop (PLL) [26]–[28].

A. IBVM Mathematical Model

To define the mathematical model of the IBVM power converter, we assume in Fig. 1 that the state vector $\boldsymbol{x} = [i_{L1}\ i_{L2}\ v_{C1}\ v_{C2}\ v_{dc\_link}]^T$ is composed by the current of the inductors (i_{L1} and i_{L2}), the voltage of the doubler cells (v_{C1} and v_{C2}) and the dc-link voltage (v_{dc_link}). The input vector $\boldsymbol{u} = [v_{fc}\ \ i_0]^T$ is composed by the FC voltage and the dc-current of the load (i_0) (VSI equivalent model) with the VSI equivalent resistance defined by $R_O = v_{dc\_link}/i_0$. In addition, the output vector $\boldsymbol{y} = [i_{L1} + i_{L2}\ v_{dc\_link}]^T$ is a function of the FC current $(i_{fc} = i_{L1} + i_{L2})$ and the dc-link voltage.

In this context, each switching interval $(k_1 \ldots k_4)$ has its mathematical model given by [29], while the IBVM model is achieved by applying the superposition theory, i.e. multiplying the state, input, output and feedforward matrices of an $\boldsymbol{i}^{th}$ subinterval ($\boldsymbol{A_i}, \boldsymbol{B_i}, \boldsymbol{C_i}$ and $\boldsymbol{D_i}$) by an $\boldsymbol{i}^{th}$ duty-cycle (k_i).

Considering that the MOSFETs are commuting with 180° of displacement, the interval in which the S_1 or S_2 stay off is $(1-k)T_S$. In this type of simplification, we obtain as result $k_1T_S + k_2T_S = 1/2\,T_S$ and $k_3T_S + k_4T_S = 1/2\,T_S$, i.e. k_2 and k_4 are equal to $(1-k)$, $k_1 = k_3 = 1/2 - (1-k) = k - 1/2$ and the state matrix takes the form:

$$\boldsymbol{A} = \sum_{i=1}^{4} \boldsymbol{A_i}\, k_i = \boldsymbol{A_1}\left(k - \tfrac{1}{2}\right) + \boldsymbol{A_2}(1-k) + \boldsymbol{A_3}\left(k - \tfrac{1}{2}\right) + \boldsymbol{A_4}(1-k) = (-\boldsymbol{A_1} + \boldsymbol{A_2} + \boldsymbol{A_4}) + k(2\boldsymbol{A_1} - \boldsymbol{A_2} - \boldsymbol{A_4}) \quad (1)$$

Consequently, substituting (1) in the state-space model and taking into account that $\boldsymbol{B} = \sum_{i=1}^{4} \boldsymbol{B_i}\, k_i = \boldsymbol{B_1}$ and $\boldsymbol{D} = 0$, the following IBVM average model illustrated in Fig. 1 is achieved:

$$\begin{cases}\dot{\boldsymbol{x}} = [(-\boldsymbol{A_1}+\boldsymbol{A_2}+\boldsymbol{A_4})+k(2\boldsymbol{A_1}-\boldsymbol{A_2}-\boldsymbol{A_4})]\boldsymbol{x}+\boldsymbol{Bu}\\ \boldsymbol{y}=\boldsymbol{Cx}\end{cases} \quad (2)$$

Considering the duty-cycle as the input variable, we apply the small-signal analysis in (2) to find the average model presented as follows:

$$\begin{cases}\dot{\boldsymbol{X}}+\dot{\hat{\boldsymbol{x}}}=\\ [(-\boldsymbol{A_1}+\boldsymbol{A_2}+\boldsymbol{A_4})+(K+\hat{k})(2\boldsymbol{A_1}-\boldsymbol{A_2}-\boldsymbol{A_4})](\boldsymbol{X}+\hat{\boldsymbol{x}})\\ +\boldsymbol{B}(\boldsymbol{U}+\hat{\boldsymbol{u}})\\ \boldsymbol{Y}+\hat{\boldsymbol{y}}=\boldsymbol{C}(\boldsymbol{X}+\hat{\boldsymbol{x}})\end{cases} \quad (3)$$

In the analysis, the input, output, state variables and the duty-cycle are evaluated considering the ac (small-signals) and dc (steady-state regime) components $\boldsymbol{u}=\boldsymbol{U}+\hat{\boldsymbol{u}}$, $\boldsymbol{y}=\boldsymbol{Y}+\hat{\boldsymbol{y}}$, $\boldsymbol{x}=\boldsymbol{X}+\hat{\boldsymbol{x}}$ and $k=K+\hat{k}$, where the uppercase denotes the steady-state regime, and the circumflex accent means the small-signal perturbation around the quiescent operating point.

In (3) the gradient of the state vector at steady-state regime is zero $(\dot{\boldsymbol{X}}=0)$, $\boldsymbol{X}=-\boldsymbol{A_n}^{-1}\boldsymbol{BU}$, $\boldsymbol{A_n}=(-\boldsymbol{A_1}+\boldsymbol{A_2}+\boldsymbol{A_4})+K(2\boldsymbol{A_1}-\boldsymbol{A_2}-\boldsymbol{A_4})$, and $\boldsymbol{F}=(2\boldsymbol{A_1}-\boldsymbol{A_2}-\boldsymbol{A_4})\boldsymbol{X}$. Finally, the ac-model of the IBVM converter is found according to:

$$\begin{cases}\dot{\hat{\boldsymbol{x}}}=[(-\boldsymbol{A_1}+\boldsymbol{A_2}+\boldsymbol{A_4})+K(2\boldsymbol{A_1}-\boldsymbol{A_2}-\boldsymbol{A_4})]\hat{\boldsymbol{x}}\\ \quad +\boldsymbol{B}\hat{\boldsymbol{u}}+(2\boldsymbol{A_1}-\boldsymbol{A_2}-\boldsymbol{A_4})\boldsymbol{X}\hat{k}\\ \hat{\boldsymbol{y}}=\boldsymbol{C}\hat{\boldsymbol{x}}\end{cases} \quad (4)$$

To simplify the ac-model defined in (4), $\boldsymbol{F}$ is incorporated in $\boldsymbol{B}$ to produce a new matrix $\boldsymbol{B'}=[\boldsymbol{B}\quad\boldsymbol{F}]$. In the same way, $\hat{k}$ is incorporated in the input vector $\hat{\boldsymbol{u}}$ to produce a new input vector $\hat{\boldsymbol{u}}'=[\hat{\boldsymbol{u}}\quad\hat{k}]^T$, as seen in:

$$\begin{cases}\dot{\hat{\boldsymbol{x}}}=\boldsymbol{A_n}\hat{\boldsymbol{x}}+\boldsymbol{B}\hat{\boldsymbol{u}}+\boldsymbol{F}\hat{k}=\boldsymbol{A_n}\hat{\boldsymbol{x}}+[\boldsymbol{B}\quad\boldsymbol{F}]\begin{bmatrix}\hat{\boldsymbol{u}}\\ \hat{k}\end{bmatrix}=\boldsymbol{A_n}\hat{\boldsymbol{x}}+\boldsymbol{B'}\hat{\boldsymbol{u}}'\\ \hat{\boldsymbol{y}}=\boldsymbol{C}\hat{\boldsymbol{x}}\end{cases} \quad (5)$$

B. Mathematical Model of the Bidirectional Converter

The mathematical model of the bidirectional power converter is achieved when we assume in Fig. 1 that the state vector $\boldsymbol{x_{ss}}=\begin{bmatrix}v_{dc\_link} & v_{Css} & i_{Lss}\end{bmatrix}^T$ is composed by the dc-link voltage, the voltage on the capacitor terminals (C_{ss}) and the inductor current (i_{Lss}). Using the same idea, the input vector $\boldsymbol{u_{ss}}=[i_0\quad v_{ss}]^T$ is composed by the voltage on the SS terminals, and the VSI is modeled as a current source (i_0).

Therefore, we calculate the state-space model switching-on and off S_3 (buck mode) and S_4 (boost mode) to produce the states matrices $\boldsymbol{A_5}$ and $\boldsymbol{A_6}$, input matrices $\boldsymbol{B_5}$ and $\boldsymbol{B_6}$, output matrices $\boldsymbol{C_5}$ and $\boldsymbol{C_6}$, and feedforward matrices $\boldsymbol{D_5}$ and $\boldsymbol{D_6}$ of each interval of switching, as follows:

$$\begin{cases}\dot{\boldsymbol{x_{ss}}}=[\boldsymbol{A_5}m_{ss}+\boldsymbol{A_6}(1-m_{ss})]\boldsymbol{x_{ss}}+\\ \quad +[\boldsymbol{B_5}m_{ss}+\boldsymbol{B_6}(1-m_{ss})]\boldsymbol{u}_{ss}\\ \boldsymbol{y_{ss}}=[\boldsymbol{C_5}m_{ss}+\boldsymbol{C_6}(1-m_{ss})]\boldsymbol{x_{ss}}+\\ \quad +[\boldsymbol{D_5}m_{ss}+\boldsymbol{D_6}(1-m_{ss})]\boldsymbol{u_{ss}}\end{cases} \quad (6)$$

Additionally, (6) needs to represent the overall mathematical model of the bidirectional dc/dc converter, i.e. when we have the boost model the duty-cycle (k_{ss}) ponders the matrix $\boldsymbol{A_5}$, $\boldsymbol{B_5}$, $\boldsymbol{C_5}$ and $\boldsymbol{D_5}$, while $(1-k_{ss})$ multiply $\boldsymbol{A_6}$, $\boldsymbol{B_6}$, $\boldsymbol{C_6}$ and $\boldsymbol{D_6}$. Moreover in the step-down mode $\boldsymbol{A_5}$, $\boldsymbol{B_5}$, $\boldsymbol{C_5}$ and $\boldsymbol{D_5}$ are multiplied by $(1-k_{ss})$ and $\boldsymbol{A_6}$, $\boldsymbol{B_6}$, $\boldsymbol{C_6}$ and $\boldsymbol{D_6}$ by k_{ss}. To generalize the model, we introduce a new variable $m_{ss}=k_{ss}$ when the boost mode is active and $m_{ss}=1-k_{ss}$ when buck mode is active, respectively.

In this context, we apply the small-signal analysis in (6) to represent the ac and dc-models $\boldsymbol{u_{ss}}=\boldsymbol{U_{ss}}+\hat{\boldsymbol{u}}_{ss}$, $\boldsymbol{y_{ss}}=\boldsymbol{Y_{ss}}+\hat{\boldsymbol{y}}_{ss}$, $\boldsymbol{x_{ss}}=\boldsymbol{X_{ss}}+\hat{\boldsymbol{x}}_{ss}$ and $m_{ss}=M_{ss}+\hat{m}_{ss}$, where the uppercase also denotes the steady-state regime, and the circumflex accent represents the small-signal perturbation around the quiescent point:

$$\begin{cases}\dot{\hat{\boldsymbol{x}}}_{ss}=\underbrace{\boldsymbol{A_{ss}X_{ss}}+\boldsymbol{B_{ss}U_{ss}}}_{=0}+\boldsymbol{A_{ss}}\hat{\boldsymbol{x}}_{ss}+\boldsymbol{R}\hat{m}_{ss}+\boldsymbol{B_{ss}}\hat{\boldsymbol{u}}_{ss}\\ \boldsymbol{Y_{ss}}+\hat{\boldsymbol{y}}_{ss}=\underbrace{\boldsymbol{C_{ss}X_{ss}}+\boldsymbol{D_{ss}U_{ss}}}_{=Y_{ss}}+\boldsymbol{C_{ss}}\hat{\boldsymbol{x}}_{ss}+\boldsymbol{Q}\hat{m}_{ss}+\boldsymbol{D_{ss}}\hat{\boldsymbol{u}}_{ss}\end{cases} \quad (7)$$

In (7) $\boldsymbol{A_{ss}}=\boldsymbol{A_5}M_{ss}+\boldsymbol{A_6}(1-M_{ss})$, $\boldsymbol{R}=(\boldsymbol{A_5}-\boldsymbol{A_6})\boldsymbol{X_{ss}}+(\boldsymbol{B_5}-\boldsymbol{B_6})\boldsymbol{U_{ss}}$, $\boldsymbol{B_{ss}}=\boldsymbol{B_5}M_{ss}+\boldsymbol{B_6}(1-M_{ss})$, $\boldsymbol{C_{ss}}=\boldsymbol{C_5}M_{ss}+\boldsymbol{C_6}(1-M_{ss})$, $\boldsymbol{Q}=(\boldsymbol{C_5}-\boldsymbol{C_6})\boldsymbol{X_{ss}}$ and $\boldsymbol{D_{ss}}=\boldsymbol{D_5}=\boldsymbol{D_6}=0$. Additionally, the steady-state regime can be represented by $\boldsymbol{X_{ss}}=-\boldsymbol{A_{ss}}^{-1}\boldsymbol{B_{ss}U_{ss}}$ $(\dot{\boldsymbol{X}}_{\boldsymbol{ss}}=0)$ and $\boldsymbol{Y_{ss}}=\boldsymbol{C_{ss}X_{ss}}$, respectively. Therefore, the ac-model of the directional power converter is calculated according to:

$$\begin{cases}\dot{\hat{\boldsymbol{x}}}_{ss}=\boldsymbol{A_{ss}}\hat{\boldsymbol{x}}_{ss}+\boldsymbol{R}\hat{m}_{ss}+\boldsymbol{B_{ss}}\hat{\boldsymbol{u}}_{ss}\\ \hat{\boldsymbol{y}}_{ss}=\boldsymbol{C_{ss}}\hat{\boldsymbol{x}}_{ss}+\boldsymbol{Q}\hat{m}_{ss}\end{cases} \quad (8)$$

III. POWER-SHARING MODELING AND CONTROL

Based on the proposed management method, the load step required from the ac-side has to be compensated by the dc microgrid as fast as possible. However, this type of transient produces stability drawbacks because of the slow-time response of the FCs. Considering the slow dynamics of the FCs and power quality problems, a set of SSs is included in the dc microgrid to compensate the load demand connected to the ac-side, as illustrated Fig. 2.

In this context, the total power available on the dc-side has to be supplied by the SS and FC:

$$p_{dc}=p_{SS}+p_{fc}+p_{losses} \quad (9)$$

where p_{dc} is the instantaneous power available on the dc-side, p_{fc} is the instantaneous power produced by the FC, p_{ss} is the instantaneous power produced by or absorbed from the SSs, while p_{losses} are the converter losses, as well.

Moreover, in Fig. 2 we observe that p_{ss} and p_{fc} are weighted by a filter transfer function because they have different dynamic response. In terms of frequency response, the power produced by the dc sources and exchanged by the SSs are complementary, i.e. the SS is weighted by a high-pass filter $(1-n_d)$ while the FC is weighted by a low-pass filter (n_d) as:

$$p_{dc}=(1-n_d)p_{ss}+n_d p_{fc} \quad (10)$$

In other words, the filter transfer function compensates the converter losses, i.e. (9) must be equal to (10). To generalize

This article has been accepted for publication in a future issue of this journal, but has not been fully edited. Content may change prior to final publication. Citation information: DOI 10.1109/TIE.2019.2916312, IEEE Transactions on Industrial Electronics

the mathematical model, we include the ac-side in the problem (Fig. 2.a). In this case, the dc-link power balance (p_{link}) is achieved when the power demanded by the ac-side (p_{pcc}) is completely produced by the dc-side (p_{dc}) as shown in:

$$p_{link} = p_{dc} - p_{pcc} \tag{11}$$

Substituting (10) into (11), we obtain the following instantaneous power model to represent the dc microgrid:

$$p_{link} = (1 - n_d)p_{SS} + n_d p_{fc} - p_{pcc} \tag{12}$$

Therefore, we can define the low-pass filter transfer function ($n_d(s)$). In order to respect the FC slow dynamics response and to prevent damage in the FC, the time-constant (τ) is designed according to the characteristics of a specific FC as follows:

$$n_d(s) = \frac{1}{s\tau + 1} \tag{13}$$

As a final point, in the scenario presented in Fig. 2.b the SS shares power only during the transitory regime, while the FC is in-charge of the steady-state regime.

A. Modelling dc/dc Converters for Power-Sharing Operation

From the mathematical model described in sections II.A and B (model of both dc/dc converters), we propose a control diagram with power-sharing dynamics as shown in Fig. 3. In this figure, H_v, H_i and H_{iss} represent the sensor gains of the dc-link voltage, the FC and SS current sensors, as well as the proportional-integral (PI) regulator P_I_v, P_I_{iss} and P_I_{ifc} for controlling the dc-link voltage, FC and SS current, respectively. Also in Fig. 3, we show the ac-voltage and current references of the dc-link ($\hat{v}_{dc\_link\_ref}$), FC ($\hat{\imath}_{fc\_ref}$) and SS ($\hat{\imath}_{Lss\_ref}$), respectively.

To calculate the FC and the SS current references (ac-components to keep the microgrid stable), we process the total current available on the dc-link ($\hat{\imath}_e(s)$) through the low-pass filter transfer function to give the FC a slower dynamics (14) and $\hat{\imath}_e(s)$ through the complementary function to obtain a faster dynamics on the SS terminals:

$$\begin{cases} \hat{\imath}_{fc\_ref}(s) = \hat{\imath}_e(s) n_d(s) \\ \hat{\imath}_{fc\_ref}(s) = \hat{\imath}_e(s) \dfrac{1}{s\tau + 1} \end{cases} \tag{14}$$

$$\begin{cases} \hat{\imath}_{Lss\_ref}(s) = \hat{\imath}_e(s)\left(1 - n_d(s)\right) \\ \hat{\imath}_{Lss\_ref}(s) = \hat{\imath}_e(s)\left(1 - \dfrac{1}{s\tau + 1}\right) \end{cases} \tag{15}$$

In Fig. 3, we show the capability of each converter to compensate the voltage deviation on the dc-link, i.e. the effect of the FC current ($\hat{\imath}_{fc\_ref}$) and the SS current ($\hat{\imath}_{Lss\_ref}$) references on the dc-link voltage ($\hat{v}_{dc\_link\_ref}$). Firstly, we calculate the current model in the closed-loop for the FC via a simple arithmetic of blocks in the time-domain when the output vector $\boldsymbol{C_i} = [1\ 1\ 0\ 0\ 0]$, such as:

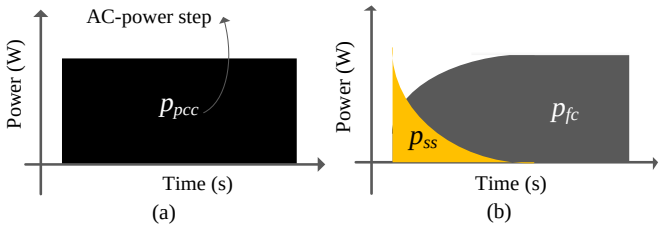

Fig. 2. Power management strategy to the transitory regime (a) ac-side and (b) dc-side.

$$\dot{\hat{\boldsymbol{x}}} = \boldsymbol{A_n}\hat{\boldsymbol{x}} + \boldsymbol{B}\hat{\boldsymbol{u}} - H_i P\_I_{i_{fc}} \boldsymbol{F C_i}\hat{\boldsymbol{x}} + P\_I_{i_{fc}} \boldsymbol{F}\hat{\imath}_{fc\_ref} \tag{16}$$

Later, we apply the Laplace's transform in (16), and make the ac-input vector equal to zero ($\hat{\boldsymbol{u}}(s) = 0$) to find the closed-loop transfer function expressed as:

$$\boldsymbol{G_{c_i}}(s) = \frac{\hat{\boldsymbol{x}}(s)}{\hat{\imath}_{fc\_ref}(s)} = \Big(s\boldsymbol{I} - \boldsymbol{A_n} + H_i P\_I_{i_{fc}}(s)\boldsymbol{F C_i}\Big)^{-1} P\_I_{i_{fc}}(s)\boldsymbol{F} \tag{17}$$

However, our goal is the FC current effect on the dc-link voltage. Taking into account that $\boldsymbol{G_{c_i}}(s)$ is a relationship between $\hat{\imath}_{fc\_ref}(s)$ and $\hat{\boldsymbol{x}}(s)$, the final objective is achieved multiplying $\hat{\boldsymbol{x}}(s)$ by a specific output vector $\boldsymbol{C_v} = [0\ 0\ 0\ 0\ 1]$ according to:

$$\frac{\hat{v}_{dc\_link}(s)}{\hat{\imath}_{fc\_ref}(s)} = \boldsymbol{C_v G_{c_i}}(s) \tag{18}$$

We adopt a similar procedure to the SS, i.e. we also compute the current model in closed-loop for the SS ($i_{Lss}(s)$) via Fig. 3, arithmetic of blocks and considering in (8) that $\boldsymbol{C_{ssi}} = \boldsymbol{C_5} = \boldsymbol{C_6} = [0\ 0\ 1]$ in the time-domain (19).

$$\dot{\hat{\boldsymbol{x}}} = \boldsymbol{A_{ss}}\hat{\boldsymbol{x}}_{\boldsymbol{ss}} + \boldsymbol{B_{ss}}\hat{\boldsymbol{u}}_{ss} + P_{I_{i_{ss}}}\boldsymbol{R}\hat{\imath}_{Lss_{ref}} - H_{iss}P_{I_{i_{ss}}}\boldsymbol{R C_{ssi}}\hat{\boldsymbol{x}}_{ss} \tag{19}$$

In addition, the output vectors in (8) are the same, i.e. $\boldsymbol{Q} = (\boldsymbol{C_5} - \boldsymbol{C_6})\boldsymbol{X_{ss}} = 0$. Later, we apply the Laplace's transform in (19), and make the ac-input vector equal to zero ($\hat{\boldsymbol{u}}_{\boldsymbol{ss}}(s) = 0$) to find the SS transfer function $\boldsymbol{G_{Css_i}}(s)$ defined in:

$$\boldsymbol{G_{Css_i}}(s) = \frac{\hat{\boldsymbol{x}}_{\boldsymbol{ss}}(s)}{\hat{\imath}_{Lss\_ref}(s)} = \Big(s\boldsymbol{I_{ss}} - \boldsymbol{A_{ss}} + H_{iss}P\_I_{i_{ss}}(s)\boldsymbol{R C_{ssi}}\Big)^{-1} P\_I_{i_{ss}}(s)\boldsymbol{R} \tag{20}$$

As previously shown, the main objective is the influence of the SS current reference on the dc-link voltage, such as:

$$\frac{\hat{v}_{dc\_link}(s)}{\hat{\imath}_{Lss\_ref}(s)} = \boldsymbol{C_{ssv}}\boldsymbol{G_{Css_i}}(s) \tag{21}$$

i.e. we ponder the vector $\hat{\boldsymbol{x}}_{\boldsymbol{ss}}(s)$ by the output vector when $\boldsymbol{C_{ssv}} = [1\ 0\ 0]$ to get as result the dc-link voltage $\hat{v}_{dc\_link}(s) = \boldsymbol{C_{ssv}}\hat{\boldsymbol{x}}_{\boldsymbol{ss}}(s)$.

After reducing the FC and SS current loops to specific

This article has been accepted for publication in a future issue of this journal, but has not been fully edited. Content may change prior to final publication. Citation information: DOI 10.1109/TIE.2019.2916312, IEEE Transactions on Industrial Electronics

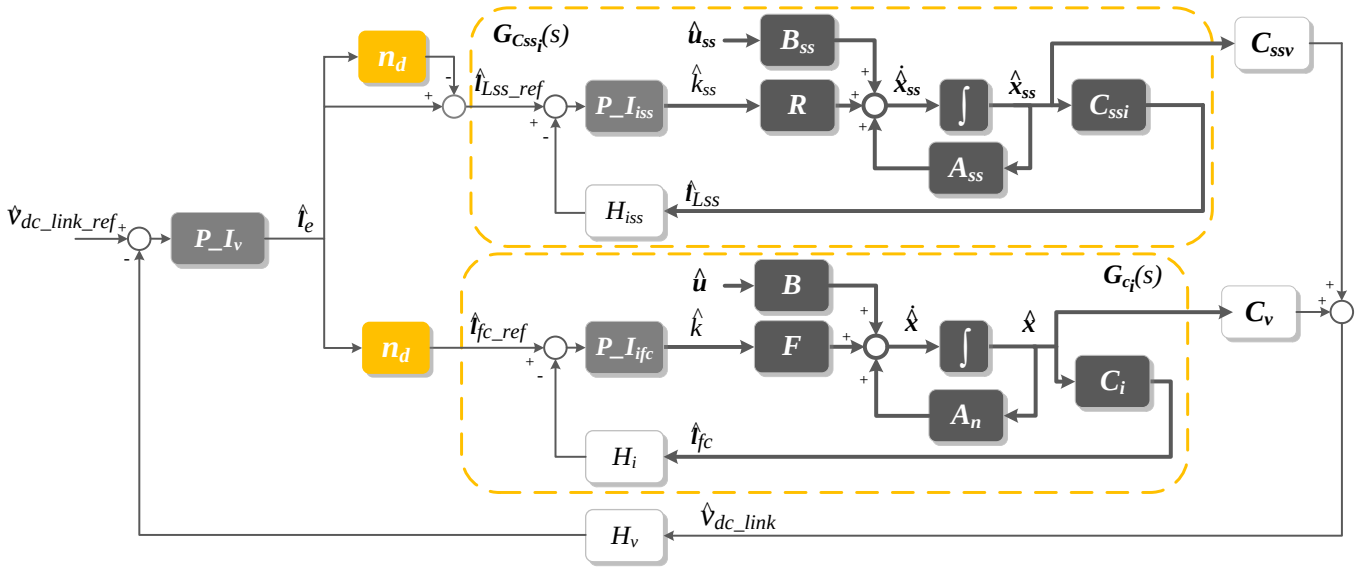

Fig. 3. Dc-link voltage control for dynamic power-sharing during transition.

transfer functions (18) and (21), we estimate the stability of the dc-link voltage loop when a PI controller is used and calculate via theory of superposition the following open-loop transfer function:

$$H_v P\_I_v(s) n_d(s) \boldsymbol{C_v G_{c_i}}(s) + H_v P\_I_v(s)(s)\big(1 - n_d(s)\big)\boldsymbol{C_{ssv} G_{Css_i}}(s) = H_v \left[k_{p_v} \frac{\left(\frac{k_{i_v}}{k_{p_v}}+s\right)}{s}\right]\left(\frac{1}{s\tau+1}\right)\boldsymbol{C_v}\Bigg(s\boldsymbol{I} - \boldsymbol{A_n} + H_i\left[k_{p_{fc}} \frac{\left(\frac{k_{i_{fc}}}{k_{p_{fc}}}+s\right)}{s}\right]\boldsymbol{F C_i}\Bigg)^{-1}\left[k_{p_{fc}} \frac{\left(\frac{k_{i_{fc}}}{k_{p_{fc}}}+s\right)}{s}\right]\boldsymbol{F} + H_v\left[k_{p_v} \frac{\left(\frac{k_{i_v}}{k_{p_v}}+s\right)}{s}\right]\left(1 - \frac{1}{s\tau+1}\right)\boldsymbol{C_{ssv}}\Bigg(s\boldsymbol{I_{ss}} - \boldsymbol{A_{ss}} + H_{iss}\left[k_{p_{ss}} \frac{\left(\frac{k_{i_{ss}}}{k_{p_{ss}}}+s\right)}{s}\right]\boldsymbol{R C_{ssi}}\Bigg)^{-1}\left[k_{p_{ss}} \frac{\left(\frac{k_{i_{ss}}}{k_{p_{ss}}}+s\right)}{s}\right]\boldsymbol{R} \quad (22)$$

where k_{p_v}, $k_{p_{fc}}$ and $k_{p_{ss}}$ are the proportional gains, and k_{i_v}, $k_{i_{fc}}$ and $k_{i_{ss}}$ are the integral gains of the voltage (dc-link) and current (FC and SS) controllers.

B. Adaptive k-Sharing

In general, the SSs are in-charge only during the transitory regime in classical operations of dc microgrids. In a modern scenario, the SS could assume an additional functionality as power production at steady-state regime as illustrated in Fig. 4. However, this task must be performed during a predefined interval of time to avoid the SS depth discharging and consequently its permanent damage in the case of batteries.

In this case, we proposed the adaptive *k*-sharing function shown in Fig. 5. This solution is based on the inclusion of an adaptive *k*-sharing function and *k*-sharing gains (k_{ps}, k_s) to manage the steady-state power absorbed from or supplied by the SS:

$$k_s = \frac{2}{1 + e^{k_{ps}\Delta\hat{v}_{link}}} \quad (23)$$

In Fig. 2.b, the *k*-sharing gain (k_s) is set to one and the SS shares power only during the transitory regime. On the other hand, in Fig. 4b the *k*-sharing gain (k_s) assumes different values of one and the SS operation mode is improved allowing it to absorb or deliver power also at steady-state regime. Unfortunately, as aforementioned this state of operation has to be managed accurately to prevent depth-of-discharge levels.

Therefore, when $k_s = 1$ the function (23) is linearized and the SSs will work only during the transients. However, when *k*-sharing gain $k_s \neq 1$, besides mitigating the transient and improving the SS response to keep the dc-link voltage stable, the *k*-sharing function also regulates the steady-state power (absorbed or delivered) by the SS to the dc-link. Thus, the variable k_s is related to the amount of power shared by the SS at steady-state regime.

In the *k*-sharing function (23), the k_{ps} gain is responsible for changing the k_s value dynamically, as shown in Fig. 6, which is associated to the dc microgrid stability. Additionally, Fig. 6 shows that for higher k_{ps} gain values, the power sharing dynamics is faster. At the same time, with increasing k_{ps} gains, the dc-link voltage error at steady-state regime is lower, because the dynamic behavior to reach the required k_s value is enhanced as illustrated in (23) and in Fig. 6.

The SS current reference $\hat{\imath}_{Lss\_ref}(s)$ is calculated taking into account the definition shown in (15), and weighting $n_d(s)$ by k_s as in:

$$\hat{\imath}_{Lss\_ref}(s) = \hat{\imath}_e(s)[1 - k_s n_d(s)] \quad (24)$$

Substituting (23) in (24) we get as result the final mathematical mode to calculate the SS current reference:

This article has been accepted for publication in a future issue of this journal, but has not been fully edited. Content may change prior to final publication. Citation information: DOI 10.1109/TIE.2019.2916312, IEEE Transactions on Industrial Electronics

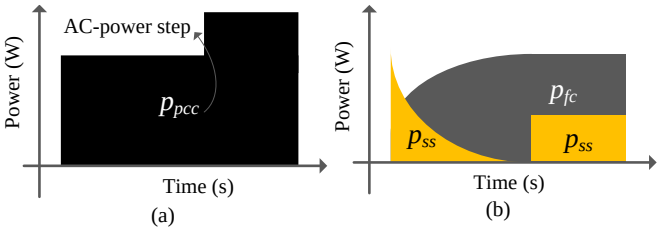

Fig. 4. Power management strategy to the transitory and steady-state regimes (a) ac-side and (b) dc-side.

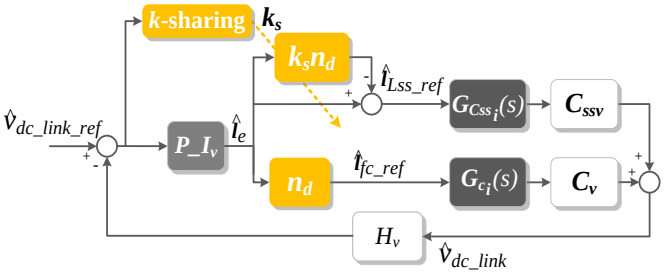

Fig. 5. Dc-link voltage control structure for dynamic *k*-sharing during the transitory and steady-state regimes.

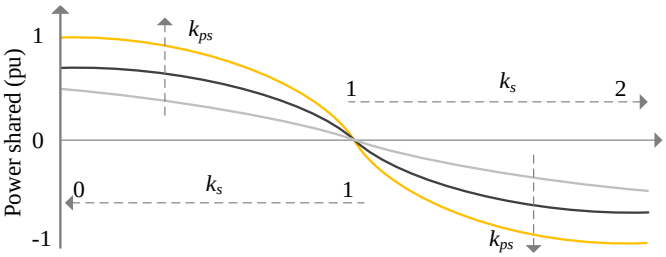

Fig. 6. Adaptive *k*-sharing operation.

$$\hat{i}_{Lss\_ref}(s) = \hat{i}_e(s)\left[1 - \left(\frac{2}{1 + e^{k_{ps}\Delta\hat{v}_{link}}}\right)\left(\frac{1}{s\tau + 1}\right)\right] \quad (25)$$

A similar analysis is performed on the FC current reference, considering the model in (14) we also multiply $n_d(s)$ by k_s to obtain the FC current reference (26). Finally, we apply (23) in (26) to get the final model of the FC current reference in:

$$\hat{i}_{fc\_ref}(s) = \hat{i}_e(s)[k_s n_d(s)] \quad (26)$$

$$\hat{i}_{fc\_ref}(s) = \hat{i}_e(s)\left[\left(\frac{2}{1 + e^{k_{ps}\Delta\hat{v}_{link}}}\right)\left(\frac{1}{s\tau + 1}\right)\right] \quad (27)$$

In Fig. 7 we plot the effect of the dc-voltage error and k_{ps} on k_s $\left[k_s f\left(\Delta\hat{v}_{link}, k_{ps}\right)\right]$. If $\Delta\hat{v}_{link} \neq 0$ and with high k_{ps} values, low $\Delta\hat{v}_{link}$ values will speed-up the power-sharing. Moreover, if $\Delta\hat{v}_{link} \neq 0$ and small values of k_{ps}, the control structure will show slow power-sharing responses. Unfortunately, the proposed approach will implicate in dc-link voltage error while the *k*-sharing technique is active. However, we reduce the deviation to less than 1.4% with an accurate adjustment of k_{ps}.

IV. Dynamic Response of the DC MicroGrid

Initially, we linearize the adaptive *k*-sharing function (23) in Fig. 3, imposing fixed k_s values for

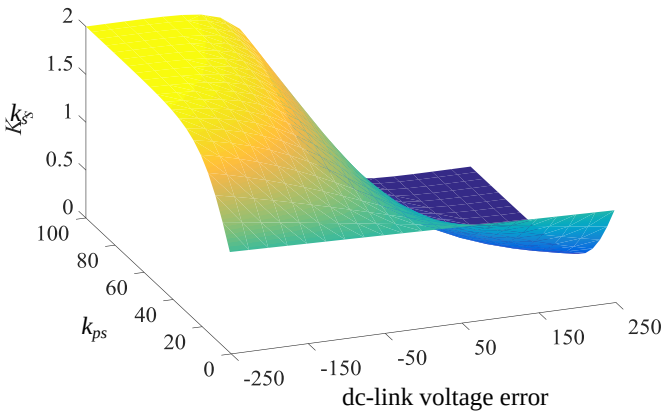

Fig. 7. The dc-link voltage error ($\Delta\hat{v}_{link}$) and k_s for different values of k_{ps}.

$k_s f\left(\Delta\hat{v}_{link}, k_{ps}\right) = 1 - k_{ps}\Delta\hat{v}_{link}$. Later, the same procedure is applied to the dynamic *k*-sharing with predefined k_{ps} values in Fig. 5. Finally, we evaluate the microgrid parametric sensitivity for different points of operation according to the parameters shown in Table I.

A. Evaluating the Adaptive k-Sharing During the Transitory

Firstly, we accomplish the frequency and step response of the dc-link voltage as shown in Fig. 3. In this context, we realize that the phase-margin and the magnitude at low frequency (≤ 10 Hz) remain unchanged as the *k*-sharing function gain (k_s) is modified between 0.1 and 1.0, Fig. 8a.

Moreover, in the same interval of frequency the phase changes from -180º to -90º as k_s changes in the same universe of discourse (between 0.1 and 1.0). Fortunately, when the frequency is greater than 10 Hz, both the magnitude and phase are not affected as the k_s gain rises, Fig. 8a.

When the dc-link voltage is submitted to a unit step, we also realize at steady-state regime an increment of the dc-link voltage error as k_s moves straightforward to zero, Fig. 8b. In all cases, the error of amplitude is smaller than 2% proving the effectiveness of the method.

B. Evaluating the Adaptive k-Sharing at Steady-State and Transitory Regimes

Now we accomplish the frequency, root locus and step response of the dc-link voltage as shown in Fig. 5. In this procedure, we realize that the gain k_{ps} defines the management dynamics, while $\Delta\hat{v}_{link}$ indicates if the SS absorbs or delivers power to the microgrid.

According to the analysis performed in Fig. 9a, we observe that at low frequency (≤ 10 Hz) the magnitude and the phase-margin are not affected when the gain k_{ps} is changed from 0.1 to 10.0. Moreover, in the same interval of frequency, the phase changes at least -90º according to Fig. 9a.

Fortunately, when we increase the frequency, the effect of k_{ps} on the magnitude and phase are negligible. Similarly, we observe that k_{ps} does not modify the bandwidth in closed-loop (Fig. 9b).

Table I
GENERAL PARAMETERS OF THE MICROGRID

Stage	Parameter	Value
General data	dc-link voltage	250 (V)
	C_{dc_link}	1.36 (mF)
	Frequency of switching	12 (kHz)
	τ	200 (ms)
SS	Voltage/Capacity	100 (V) / 5 (Ah)
FC	Voltage/Current	28.8 (V) / 35 (A)
Buck-boost bidirectional	R_s	50 (mΩ)
	C_{ss}	940 (μF)
	$R_{C_{ss}}$	175 (mΩ)
	L_{ss}	10 (mH)
	$R_{L_{ss}}$	300 (mΩ)
IBVM	$L_1 = L_2$	870 (μH)
	$r_{L1} = r_{L2}$	34.8 (mΩ)
	$C_1 = C_2$	1 (μF)
	$r_{C1} = r_{C2}$	29 (mΩ)
AC inverter	Rated voltage (P-N)	63.5 (V)
	L_{dg}	2 (mH)
	R_{dg}	100 (mΩ)
	L_g	5 (mH)
	R_g	100 (mΩ)
	C	10 (μF)
	R_C	10 (Ω)

The stability analysis of the FC and SS are shown in Fig. 10. As the SS voltage drops, the conjugate poles approach instability, which indicate a slower response, i.e. a smaller SS capacity is needed to compensate transients, Fig. 10a. On the other hand, increasing the dynamic response of the FC no impact is performed on the power-sharing control, i.e. the *k*-sharing gain compensates the FC slow dynamics through of the SS, Fig. 10b. In this analysis, we used k_s= 0.5, i.e. there is an amount of power being shared in steady-state regime.

We also plot the step response for different k_{ps} values in Fig. 11a. In Fig. 11b (zoom of Fig. 11a), we visualize an increment of the 6% on the overshoot as k_{ps} is greater, which is predictable because high k_{ps} values reduce the damping factor and increase the dynamic response of the adaptive *k*-sharing control structure. On the other hand, when the gain k_{ps} is changed from 0.1 to 10.0 there are no substantial changes in the settling time and rise time.

V. RESULTS

A general illustration of the experimental microgrid is shown in Fig. 12. The prototype uses a 32-bits float point microprocessor (TMS28335) from Texas Instruments as logic unity, a FC H-1000 from Horizon Technologies as main source, and a set of ion-lithium-polymer as SS. In this context, we performed test to corroborate the *k*-sharing effectiveness, as well as to evaluate the capability of the proposed approach when the sharing gains are changed. Additionally, to connect the VSI to the grid, a 2 kW transformer is used as galvanic isolation at low frequency (60 Hz) in this type of prototype.

A. k-Sharing Operation

After the successful FC warming-up, a load step from 250 W to 500 W was performed on the ac-side to evaluate the effectiveness of the proposed approach.

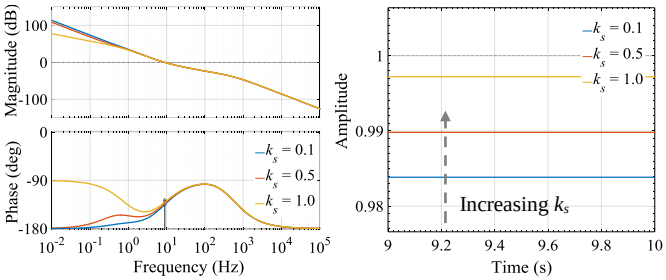

Fig. 8. Frequency response open loop (a) and unity step (b) for dc-link voltage and different k_s values.

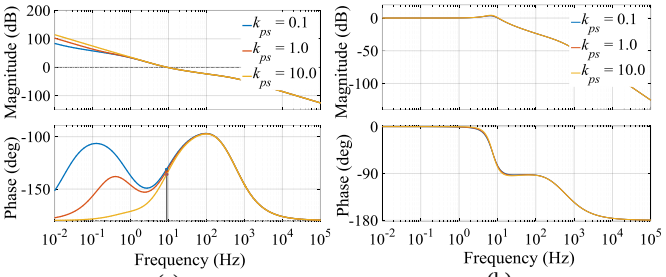

Fig. 9. Frequency response open loop (a) and closed loop (b) for dc-link voltage and different k_{ps} values.

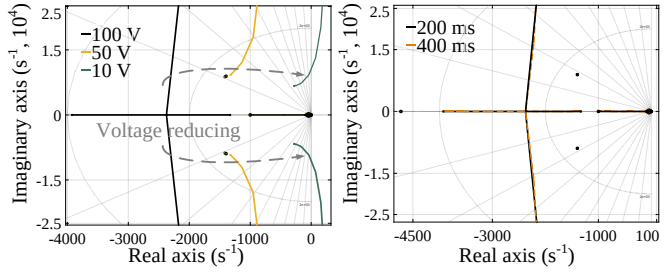

Fig. 10. Root locus (a) for different v_{ss} values and (b) different time-constant τ.

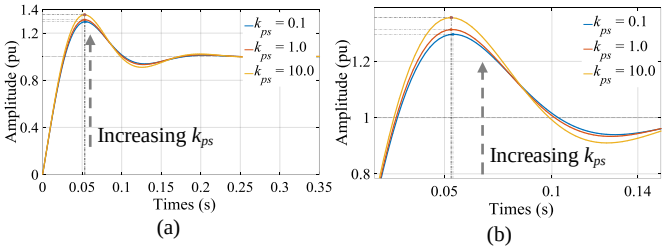

Fig. 11. Unity step behavior (a) and zoom (b) for different k_{ps} values.

In this event, the SS works only in the transients, i.e. the SS current (i_{ss}) will supply the power deficit when the load is connected, and reabsorbing it when it is removed, while the FC current (i_{fc}) will produce a slow time dynamic response caused by the chemical reaction inside the FC, Fig. 13.

Additionally, we also evaluate the power balance shown in Fig. 14, where the power step required on the ac-side (blue) produces a fast power response on the SS (orange) and a slow dynamics on the FC (pink), i.e. the SS and the FC present a complementary dynamics and an equilibrium between the ac and dc-sides.

This article has been accepted for publication in a future issue of this journal, but has not been fully edited. Content may change prior to final publication. Citation information: DOI 10.1109/TIE.2019.2916312, IEEE Transactions on Industrial Electronics

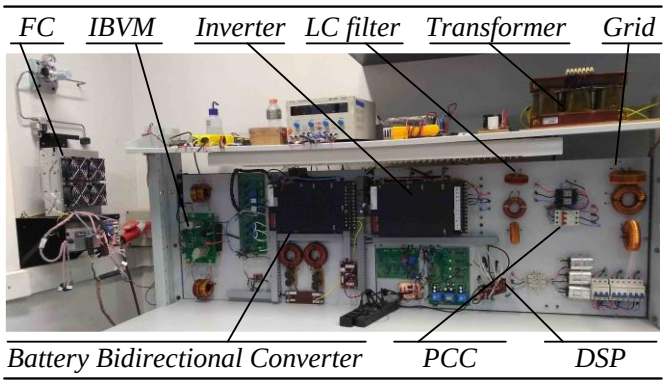

Fig. 12. Experimental setup.

Methods such as [17]–[22] focus on the study of power sharing, but do not include optimizations in relation to their power sources. As can be seen in the results of Fig. 13 and Fig. 14, the adaptive *k*-sharing function linked the FC dynamics (adjusted in τ = 200 ms) with the management of dc microgrid. This characteristic prevents damage in the FC system ensuring that the entire FC operation is performed in accordance to the characteristics of the FC.

We also evaluate the effect of the load connection and disconnection on the ac-side, in Fig. 15. In both analysis (Fig. 15b and c), we observe a fast recovery (smaller than 4 cycles of 60 Hz) of the PCC (point of common coupling) voltage (v_{pcc}) and the grid current.

In contrast, Fig. 16 shows the power management applied to the transitory and steady-state regimes. In Fig. 16, the FC delivers 250 W, while the SS does not contribute with power production to the microgrid. However, a load step is applied in the ac-side, which increases the p_{pcc} power from 250 to 500 W. Considering that $k_{ps} = 20$, the SS supplies the power deficit during the transitory. On the other hand, when the load is increased to 250 W, the *k*-sharing control modifies the SS operation point ($k_s \neq 1$) to deliver power at steady-state regime and keep the microgrid stability.

As illustrated in Fig. 16, the adaptive *k*-sharing function includes the capability of managing the power at steady-state regime, which is useful to prevent FC starvation during the initialization process. Also in this figure, we observe that the voltage deviation on the dc-link is smaller than 2% in the range of operation, as expected.

B. Evaluation of k-Sharing Gains

In Fig. 17 (a) and (b), we test the *k*-sharing stability with the gain k_{ps} = 5 and 20, respectively. In the first case, the dc-link voltage changes at most 8.5 V (3.4% of voltage error), while time response to achieve the steady-state regime is around 400 ms.

On the other hand, in the second test, we increment the k_{ps} gain in 4-times. In this type of solution, the voltage deviation is at most 3.5 V (the voltage deviation is equal to 1.4%), while time response to achieve the steady-state regime is smaller than 200 ms.

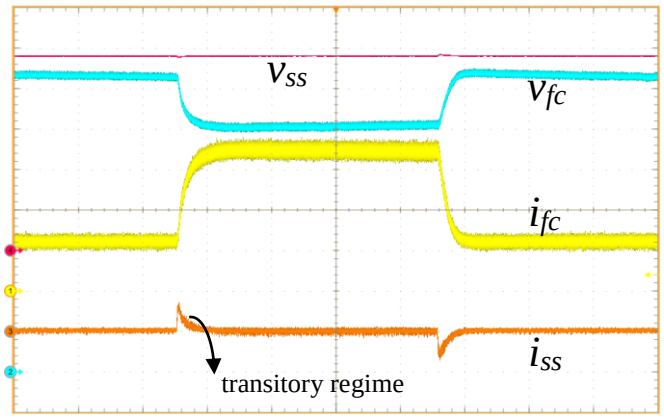

Fig. 13. Evaluation of the *k*-sharing control - transitory. Vertical: SS voltage (20 V/div.), FC voltage (5 V/div.), FC current (5 A/div.), SS current (5 A/div.). Horizontal: Time (2 s/div.).

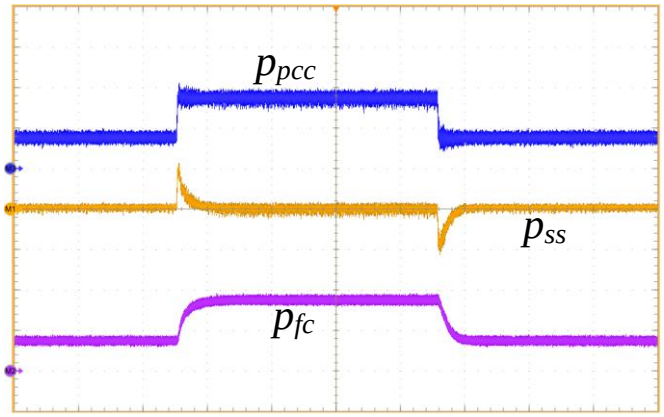

Fig. 14. Power balance - transitory. Vertical: total power (300 W/div.), SS power (300 W/div.), FC power (300 W/div.). Horizontal: Time (2 s/div.).

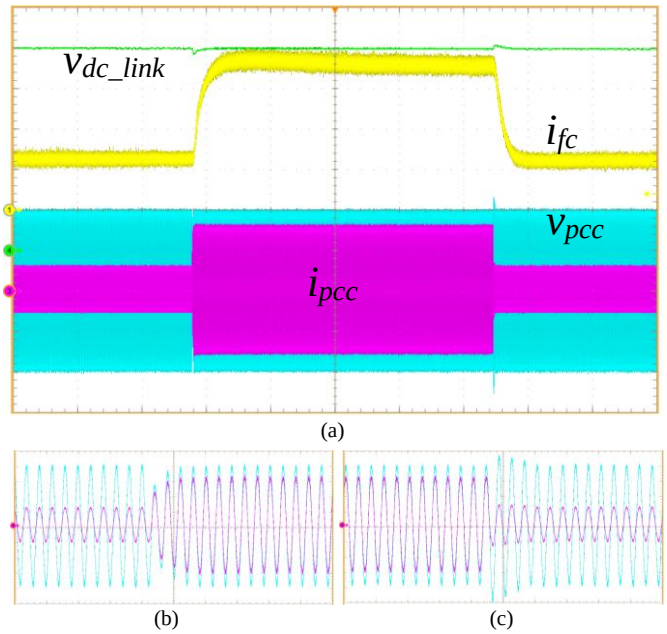

Fig. 15. Grid evaluation. (a) load connection, (b) load step and (c) load step down. Vertical: dc-link voltage (50 V/div.), FC current (5 A/div.), PCC voltage (50 V/div.), PCC current (2 A/div.). Horizontal: Time (2 s/div.).

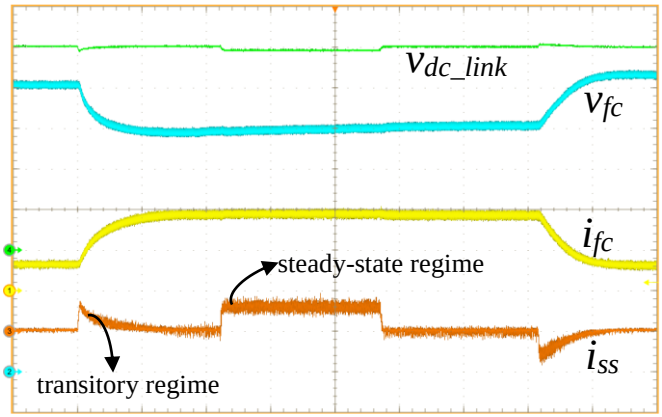

Fig. 16. Evaluation of the *k*-sharing control - transitory and steady-state regime. Vertical: dc-link voltage (50 V/div.), FC voltage (5 V/div.), FC current (10 A/div.), SS current (5 A/div.). Horizontal: Time (2 s/div.).

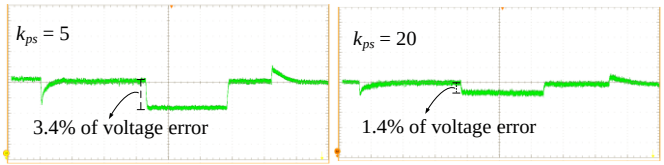

(a) (b)

Fig. 17. dc-link voltage - transitory and steady-state regime. (a) k_{ps} = 5 and (b) k_{ps} = 20. Vertical: dc-link voltage (5 V/div. Horizontal: Time (2 s/div.).

As the load maneuver is the same for both tests in Fig. 17 (a) and (b), the results show the positive impact of the k_{ps} in the dc-link voltage error.

VI. CONCLUSION

In this paper we presented an adaptive *k*-sharing method to achieve high levels of stability and improve the FC operation. To improve the dc microgrid functionality, the adaptive *k*-sharing method allows the SS to operate not only during the transitory, but also at the steady-state regime. To prevent disturbances on the FC terminals, we proposed controllers with distinct dynamic response for the FC and the SS control structures. In addition, we perform a stability analysis to determine the range of operation of the controllers when k_s is linear and nonlinear. Finally, including the *k*-sharing gain (k_{ps}), it was possible to adjust the voltage deviation and reduce de voltage error by 1.4%. For future works, tertiary control loops operating at low frequency should be used to reduce the voltage error at steady-state regime.

REFERENCES

[1] Q. Wu, Q. Wang, J. Xu, and L. Xiao, "Implementation of an Active-Clamped Current-Fed Push-Pull Converter Employing Parallel-Inductor to Extend ZVS Range for Fuel Cell Application," *IEEE Trans. Ind. Electron.*, vol. 64, no. 10, pp. 7919–7929, 2017.

[2] H. Ramírez-Murillo, C. Restrepo, J. Calvente, A. Romero, and R. Giral, "Energy Management of a Fuel-Cell Serial-Parallel Hybrid System," *IEEE Trans. Ind. Electron.*, vol. 62, no. 8, pp. 5227–5235, 2015.

[3] G. H. F. Fuzato, C. R. Aguiar, K. D. A. Ottoboni, R. F. Bastos, and R. Q. Machado, "Voltage gain analysis of the interleaved boost with voltage multiplier converter used as electronic interface for fuel cells systems," *IET Power Electron.*, vol. 9, no. 9, 2016.

[4] K. Jin, M. Yang, X. Ruan, and M. Xu, "Three-Level Bidirectional Converter for Fuel-Cell/Battery Hybrid Power System," *IEEE Trans. Ind. Electron.*, vol. 57, no. 6, pp. 1976–1986, 2010.

[5] K. Jin, X. Ruan, M. Yang, and M. Xu, "A Hybrid Fuel Cell Power System," *IEEE Trans. Ind. Electron.*, vol. 56, no. 4, pp. 1212–1222, 2009.

[6] C. R. Aguiar, G. Fuzato, R. F. Bastos, A. F. Q. Gonçalves, and R. Q. Machado, "Hybrid fuzzy anti-islanding for grid-connected and islanding operation in distributed generation systems," *IET Power Electron.*, vol. 9, no. 3, 2016.

[7] W. Garcia-Gabin, F. Dorado, and C. Bordons, "Real-time implementation of a sliding mode controller for air supply on a PEM fuel cell," *J. Process Control*, vol. 20, no. 3, pp. 325–336, 2010.

[8] J. K. Gruber, C. Bordons, and A. Oliva, "Nonlinear MPC for the airflow in a PEM fuel cell using a Volterra series model," *Control Eng. Pract.*, vol. 20, no. 2, pp. 205–217, 2012.

[9] M. Jang, M. Ciobotaru, and V. G. Agelidis, "A Single-Phase Grid-Connected Fuel Cell System Based on a Boost-Inverter," *IEEE Trans. Power Electron.*, vol. 28, no. 1, pp. 279–288, 2013.

[10] A. S. Samosir and A. H. M. Yatim, "Implementation of Dynamic Evolution Control of Bidirectional DC-DC Converter for Interfacing Ultracapacitor Energy Storage to Fuel-Cell System," *IEEE Trans. Ind. Electron.*, vol. 57, no. 10, pp. 3468–3473, 2010.

[11] W. Li, W. Li, Y. Deng, and X. He, "Single-Stage Single-Phase High-Step-Up ZVT Boost Converter for Fuel-Cell Microgrid System," *IEEE Trans. Power Electron.*, vol. 25, no. 12, pp. 3057–3065, 2010.

[12] H. Han, X. Hou, J. Yang, J. Wu, M. Su, and J. M. Guerrero, "Review of power sharing control strategies for islanding operation of AC microgrids," *IEEE Trans. Smart Grid*, vol. 7, no. 1, pp. 200–215, 2016.

[13] S. Anand, B. G. Fernandes, and J. M. Guerrero, "Distributed control to ensure proportional load sharing and improve voltage regulation in low-voltage DC microgrids," *IEEE Trans. Power Electron.*, vol. 28, no. 4, pp. 1900–1913, 2013.

[14] P. Wang, X. Lu, X. Yang, W. Wang, and D. Xu, "An Improved Distributed Secondary Control Method for DC Microgrids with Enhanced Dynamic Current Sharing Performance," *IEEE Trans. Power Electron.*, vol. 31, no. 9, pp. 6658–6673, 2016.

[15] X. Lu, J. M. Guerrero, K. Sun, and J. C. Vasquez, "An improved droop control method for dc microgrids based on low bandwidth communication with dc bus voltage restoration and enhanced current sharing accuracy," *IEEE Trans. Power Electron.*, vol. 29, no. 4, pp. 1800–1812, 2014.

[16] Y. Han, H. Li, P. Shen, E. A. A. Coelho, and J. M. Guerrero, "Review of Active and Reactive Power Sharing Strategies in Hierarchical Controlled Microgrids," *IEEE Trans. Power Electron.*, vol. 32, no. 3, pp. 2427–2451, 2017.

[17] H. Cai, J. Xiang, and W. Wei, "Decentralized Coordination Control of Multiple Photovoltaic Sources for DC Bus Voltage Regulating and Power Sharing," *IEEE Trans. Ind. Electron.*, vol. 65, no. 7, pp. 5601–5610, 2018.

[18] J. Zhou, H. Zhang, Q. Sun, D. Ma, and B. Huang, "Event-based distributed active power sharing control for interconnected AC and DC microgrids," *IEEE Trans. Smart Grid*, vol. 9, no. 6, pp. 6815–6828, 2018.

[19] Q. Xu *et al.*, "A Decentralized Dynamic Power Sharing Strategy for Hybrid Energy Storage System in Autonomous DC Microgrid," *IEEE Trans. Ind. Electron.*, vol. 64, no. 7, pp. 5930–5941, 2017.

[20] H. Kakigano, Y. Miura, and T. Ise, "Distribution voltage control for DC microgrids using fuzzy control and gain-scheduling technique," *IEEE Trans. Power Electron.*, vol. 28, no. 5, pp. 2246–2258, 2013.

[21] A. Ghazanfari, M. Hamzeh, H. Mokhtari, and H. Karimi, "Active power management of multihybrid fuel cell/supercapacitor power conversion system in a medium voltage microgrid," *IEEE Trans. Smart Grid*, vol. 3, no. 4, pp. 1903–1910, 2012.

[22] W. Jiang and B. Fahimi, "Active current sharing and source management in fuel cellbattery hybrid power system," *IEEE Trans. Ind. Electron.*, vol. 57, no. 2, pp. 752–761, 2010.

[23] J. Ma, L. Yuan, Z. Zhao, and F. He, "Transmission Loss Optimization-Based Optimal Power Flow Strategy by Hierarchical Control for DC Microgrids," *IEEE Trans. Power Electron.*, vol. 32, no. 3, pp. 1952–

1963, 2017.
[24] D. H. Dam and H. H. Lee, "A Power Distributed Control Method for Proportional Load Power Sharing and Bus Voltage Restoration in a DC Microgrid," *IEEE Trans. Ind. Appl.*, vol. 54, no. 4, pp. 3616–3625, 2018.
[25] F. Guo, Q. Xu, C. Wen, L. Wang, and P. Wang, "Distributed Secondary Control for Power Allocation and Voltage Restoration in Islanded DC Microgrids," *IEEE Trans. Sustain. Energy*, vol. 9, no. 4, pp. 1857–1869, 2018.
[26] F. Blaabjerg, R. Teodorescu, M. Liserre, and A. V Timbus, "Overview of Control and Grid Synchronization for Distributed Power Generation Systems," *IEEE Trans. Ind. Electron.*, vol. 53, no. 5, pp. 1398–1409, 2006.
[27] R. Teodorescu, F. Blaabjerg, M. Liserre, and P. C. Loh, "Proportional-resonant controllers and filters for grid-connected voltage-source converters," *Power*, vol. 153, no. 5, 2006.
[28] P. Mattavelli, "A closed-loop selective harmonic compensation for active filters," *IEEE Trans. Ind. Appl.*, vol. 37, no. 1, pp. 81–89, 2001.
[29] G. Spiazzi, S. Buso, F. Sichirollo, and L. Corradini, "Small-signal modeling of the interleaved boost with voltage multiplier," in *2012 IEEE Energy Conversion Congress and Exposition (ECCE)*, 2012, pp. 431–437.

Cassius Rossi de Aguiar was born in Santa Maria, Brazil. He received the bachelor's degree in electrical engineering from the Federal University of Santa Maria, Santa Maria, in 2008, and the master's and Ph.D. degrees in electrical engineering from the University of São Paulo, São Paulo, Brazil, in 2013 and 2016, respectively.

He is currently a Professor with the Federal University of Technology – Paraná, Toledo, Brazil. His main research interests include microgrids, energy management, and dc–dc converters for renewable and storage systems.

Guilherme Henrique Favaro Fuzato graduated in Electrical Engineering at University of São Paulo in 2011. In 2015 he received the M.S. degree in Electrical Engineering at University of São Paulo, where he is currently pursuing the Ph.D. degree. From 2018 to 2019 he was a visiting researcher at the University of Aalborg. He also works as lecturer at the Federal Institute of Education, Science and Technology of São Paulo. His main research interests are in the fields of microgrids, energy management and DC-DC converter for renewable and storage systems.

Ricardo Quadros Machado (M'05) was born in Santa Maria, Brazil. He received the Bachelor's degree from the University of Santa Maria in 1997, the Master's (2000) and the Ph.D. (2005) degrees in Electrical Engineering from the University of Campinas, Brazil. From 2002 to 2003 he was a visiting researcher at the University of Padova, Italy and from 2005 to 2007 he was a post-doctorate at the Federal University of Santa Maria. From 2013 to 2014 he was visiting professor at the University of Toronto, Canada. Additionally, from 2007 to 2018 he was assistant professor at University of São Paulo/São Carlos. Currently, he is associate professor at the same university and his main research interests are: processing of energy in dc/dc and dc/ac converters, digital control of power converters, distributed generation systems, smart grids and control of renewable energy sources.

Josep M. Guerrero (S'01–M'04–SM'08–F'15) received the B.S. degree in telecommunications engineering, the M.S. degree in electronics engineering, and the Ph.D. degree in power electronics from the Technical University of Catalonia, Barcelona, Spain, in 1997, 2000, and 2003, respectively.

Since 2011, he has been a Full Professor with the Department of Energy Technology, Aalborg University, Aalborg, Denmark, where he is responsible for the Microgrid Research Program. Since 2012, he has been a Guest Professor with the Chinese Academy of Science, Beijing, China, and the Nanjing University of Aeronautics and Astronautics, Nanjing, China; since 2014, he has been the Chair Professor with Shandong University, Jinan, China; since 2015, he has been a Distinguished Guest Professor with Hunan University, Changsha, China; and since 2016, he has been a Visiting Professor Fellow with Aston University, Birmingham, U.K. His research interests are oriented to different microgrid aspects, including power electronics, distributed energy-storage systems, hierarchical and cooperative control, energy management systems, smart metering, and the Internet of things for ac–dc microgrid clusters and islanded minigrids; current research interests are especially focused on maritime microgrids for electrical ships, vessels, ferries, and seaports.

Dr. Guerrero is an Associate Editor for the IEEE TRANSACTIONS ON POWER ELECTRONICS, the IEEE TRANSACTIONS ON INDUSTRIAL ELECTRONICS, and the IEEE INDUSTRIAL ELECTRONICS MAGAZINE, and an Editor for the IEEE TRANSACTIONS ON SMART GRID and the IEEE TRANSACTIONS ON ENERGY CONVERSION. He was the Chair of the Renewable Energy Systems Technical Committee of the IEEE Industrial Electronics Society. He was a recipient of the IEEE TRANSACTIONS ON ENERGY CONVERSION Best Paper Award for the period 2014–2015, and the Highly Cited Researcher Award by Thomson Reuters in 2014 and 2015.